**Table I.** Comparison of the MMP-13 gene expression between extrinsic and normal tendon fibroblasts six hours after cytokine stimulation

| | Mean (± SD) relative intensity ratio of MMP-13 mRNA/GAPDH mRNA | | |
|---|---|---|---|
| | Extrinsic fibroblasts | Normal fibroblasts | p-value |
| No cytokines | 2.01 ± 0.48 | 1.00 | 0.010 |
| IL-1β (10 ng/ml) | 13.88 ± 5.84* | 18.48 ± 7.34* | 0.005 |
| PDGF-BB (100 ng/ml) | 2.13 ± 0.76 | 1.41 ± 0.49 | 0.005 |
| TGF-β (10 ng/ml) | 0.36 ± 0.19* | 0.39 ± 0.14* | 0.252 |

* significantly different from the values without cytokine stimulation ($p < 0.05$)


Fig. 2a


Fig. 2b

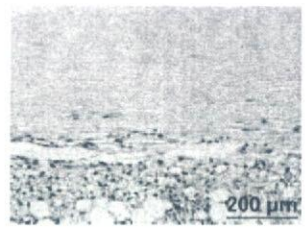


Fig. 3a

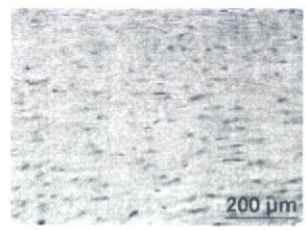


Fig. 3b


Fig. 2c


Fig. 2d

Photomicrographs showing the local expression of IL-1β in the patellar tendon a) two weeks and b) six weeks after freeze-thaw treatment and c) two and d) six weeks after the sham operation (streptavidin-biotin and haematoxylin × 100).

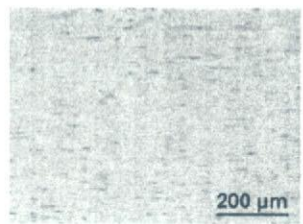


Fig. 3c

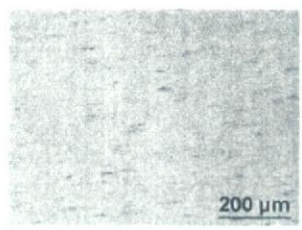


Fig. 3d

Photomicrographs showing the local expression of PDGF-BB in the patellar tendon a) two weeks and b) six weeks after freeze-thaw treatment, and c) two and d) six weeks after the sham operation (streptavidin-biotin and haematoxylin × 100).

## Discussion

Fibroblasts from an extrinsic origin repopulate the transplanted patellar tendon after fibroblast necrosis during the early phase after ligament reconstruction. These extrinsic fibroblasts remodel the graft matrix.[1-3] IL-1, PDGF, and TGF-β are known to regulate the synthesis and degradation of collagen by the fibroblasts.[5,6,9] Our study was undertaken to clarify the intrinsic response of the fibroblasts which infiltrate the necrotic patellar tendon to IL-1β, PDGF-BB, and TGF-β1 by assessing the gene expression of MMP-13. Our findings showed that fibroblasts derived from the patellar tendon six weeks after the freeze-thaw procedure had less response to IL-1β than normal tendon fibroblasts with respect to the regulation of MMP-13 mRNA. IL-1β was found to be over-expressed in the extrinsic fibroblasts which had infiltrated the necrotic patellar tendon.

We have previously compared the characteristics of extrinsic fibroblasts with those of normal tendon fibroblasts in a rabbit model.[7] In the present study we selected the rat model to obtain the antibodies for imunohistology and the probe for Northern blot analysis. Size and species differences may have affected the reliability and validity of this model. Our previous study in rats using the freeze-thaw technique *in situ* showed that this devitalised all the fibroblasts in the patellar tendon. Extrinsic fibroblasts then entirely infiltrated the patellar tendon by six weeks after freeze-thawing and they expressed more type-III collagen than the fibroblasts in the normal patellar tendon.[8] In the present study, for the Northern blot analysis we used cells derived from the patellar tendon six weeks after the freeze-thaw treatment. Immunohistological assessment showed that no cells were seen in the deep portion of the midsub-

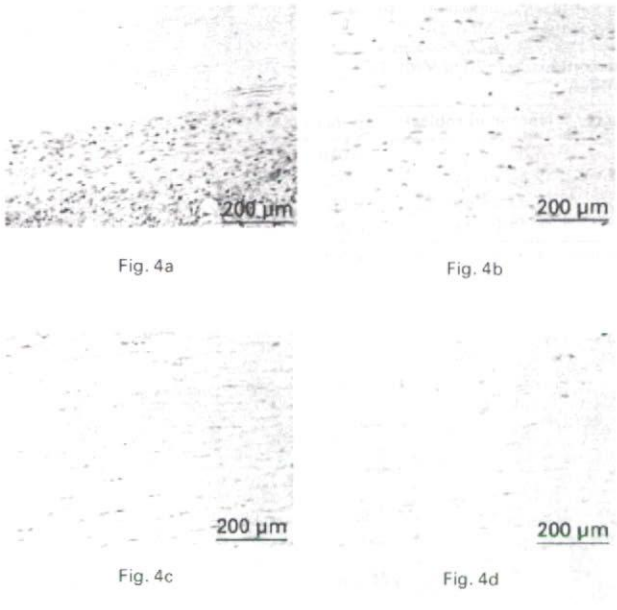


Fig. 4a

Fig. 4b

Fig. 4c

Fig. 4d

Photomicrographs showing the local expression of TGF-β in the patellar tendon a) two weeks and b) six weeks after freeze-thaw treatment and c) two and d) six weeks after the sham operation (streptavidin-biotic and haematoxylin × 100).

stance two weeks after freeze-thaw treatment, while cellular infiltration was observed at the superficial portion close to the infrapatellar fat pad. Therefore, it was difficult to isolate extrinsic fibroblasts from the patellar tendon two weeks after freeze-thaw treatment, but by six weeks, a number of fibroblasts were scattered in the tendon and we easily obtained extrinsic fibroblasts by using our tissue-explant technique.

With the Northern blot analysis, we evaluated the mRNA of MMP-13 six hours after cytokine stimulation. As shown in Figure 1b, we observed the peak of MMP-13 mRNA in response to IL-1β or PDGF stimulation six hours after stimulation. We therefore used six hours as the time point for evaluation of MMP-13 with Northern blot analysis.

Collagenases are MMPs which can initiate the cleavage of collagen fibrils at neutral pH.[9] Three collagenases have been described: collagenase 1 (MMP-1), collagenase 2 (MMP-8), and collagenase 3 (MMP-13).[9-11] MMP-1 and MMP-13 degrade type-1 collagen fibrils with similar efficiency.[9] Unlike in man, the rat expresses only one interstitial collagenase, now named MMP-13, because it has a high degree of homology of function and sequence (86%) with human MMP-13, but not with human MMP-1.[12] Consequently, MMP-13 is considered to be central to the process of collagen degradation and matrix breakdown in the rat. The present study demonstrated that IL-1β induced the gene expression of MMP-13 in extrinsic fibroblasts which were derived from the devitalised patellar tendon as well as in normal tendon fibroblasts. It is thought that tendon cells would express receptors and respond to IL-1 in an initial 'molecular inflammation' cascade, the connective tissue-cell expression of cytokines which induce matrix-destructive enzymes.[6,13] For example, Tuszaki et al[13] reported that IL-1β stimulated the MMP-1, -3, and -13 gene expression of normal human tendon cells. Their findings were consistent with those of our present study. Therefore, interstitial collagenases could be induced by IL-1 expressed by the fibroblasts infiltrating the grafted tendon, and such collagenases could then destroy the matrix of the graft during the remodelling of the grafted tendon. A previous study has shown that the expression of mRNA for collagenase in cultured fibroblasts from hypertrophic scars after skin wounds was lower than that from normal dermis.[14] Another found that no change in MMP-1 or MMP-3 could be shown with stimulation by IL-6 in hypertrophic scar fibroblasts, although mRNA and protein for MMP-1 and MMP-3 were increased by IL-6 in normal skin fibroblasts.[15] We have previously shown that extrinsic fibroblasts are phenotypically different from normal tendon fibroblasts in terms of proliferation, migration abilities and expression of integrin.[7] In the present study, we found that extrinsic fibroblasts were less stimulated by IL-1β than normal tendon fibroblasts in terms of the induction of interstitial collagenase mRNA.

Our study has shown over-expression of IL-1β in the tendon graft model, although several other authors have reported that IL-1β was over-expressed in the surrounding tissues of tendons with tendonitis.[16-19] It is recognised that the level of IL-1β released by neutrophils begins to rise rapidly after wounding and reaches a peak after several hours, suggesting that IL-1β plays an important role in the commencement of inflammation.[20,21] However, Kondo and Ohshima[22] observed a second increase in IL-1β at the proliferative stage after wounding in the rat skin, with migration of fibroblasts and the formation of new granulation tissue. We found that the extrinsic fibroblasts which were infiltrating the patellar tendon continued to over-express IL-1β for at least six weeks after necrosis of the intrinsic fibroblasts. These experimental findings indicated that IL-1β had another function with a close relationship to matrix remodelling, in addition to the commencement of inflammation during the process of tissue healing.

IL-1 is a polypeptide which is produced by macrophages, fibroblasts and neutrophils as a response to infection, injury, or antigenic challenges.[23] After trauma, IL-1β is initially produced by activated macrophages and plays an important role in the initiation of the inflammatory response. It has a close relationship to wound remodelling as well as inflammation.[22] In general, stimulation of IL-1 increases its synthesis in the autocrine and paracrine fashion and decreases the expression of IL-1 receptor.[24] Based on these findings in previous studies and the results of the present investigation, we suggest the following mechanism of the cellular response to graft integration with a cytokine/cellular control cascade for extrinsic fibroblasts during the

remodelling of the tendon after fibroblast necrosis. First, IL-1β is produced by macrophages, fibroblasts, and neutrophils surrounding the patellar tendon as a response to the invasive effects of the surgical procedure. Then the secreted IL-1β stimulates the production of collagenase by extrinsic fibroblasts during the infiltration of fibroblasts into the tendon after necrosis of the intrinsic cells. The secreted IL-1β from extrinsic fibroblasts also stimulates the production of IL-1β by the extrinsic fibroblasts themselves in the autocrine and paracrine fashion. IL-1β may reduce IL-1 receptor expression, resulting in the decrease of the responsiveness of extrinsic fibroblasts to IL-1β during the infiltration of extrinsic fibroblasts into the necrotic patellar tendon. Further study should be conducted to verify this hypothesis.

A few limitations are apparent in our study. First, we obtained infiltrative fibroblasts from the patellar tendon after a freeze-thaw treatment which had killed the intrinsic fibroblasts. However, this treatment is not identical to the conditions at tendon grafting and hence the cellular characteristics of infiltrative fibroblasts obtained in the current study may not have corresponded completely to those of fibroblasts in a grafted tendon. Secondly, we evaluated the cellular characteristics at approximately three weeks after harvesting of the patellar tendon. Although we performed only a third passage in the present study because serial passaging diminishes the differences in the phenotypical characteristics of fibroblasts, some cellular characteristics may have changed during the three weeks of culture. Previous studies have shown that the differences in the characteristics of different fibroblasts become insignificant with the serial passaging of the cells.[25,26] Therefore, the difference in the cellular response to cytokines between extrinsic and normal tendon fibroblasts may have been underestimated in this study. However, many investigators have used the cultured tendon fibroblasts from the third passage or more,[9,27,28] and we believe that our usage of cultured fibroblasts from the third passage is acceptable. Thirdly, we starved the fibroblasts of serum in the culture medium. This may have affected their differentiation, although the morphological appearances of cells before cytokine stimulation were similar to those before FBS starvation in the present experiments. In the present study we did not apply FBS 24 hours before cytokine stimulation because the existence of cytokines in FBS probably affected the response to additional cytokine stimulation. Based on previous studies,[29-31] the mean concentration of IL-1β, PDGF and TGF-β1 in human serum is approximately 2 pg/ml, 2 ng/ml and 40 ng/ml, respectively. Therefore the amounts of PDGF and TGF-β1 in FBS are not considered to be negligible compared with the amounts which we applied as cytokine stimulation. The fourth limitation is that we compared the response of extrinsic fibroblasts to cytokine stimulation in terms of MMP-13 under the condition which we had observed to have the most significant effect on cytokine stimulation of gene expression of extrinsic cells in the time-course and the dose-dependency experiments. We had no such information concerning the effect on gene expression in normal tendon fibroblasts. There is therefore, a possibility that we have overestimated the response of the extrinsic fibroblasts to cytokine stimulation in terms of MMP-13 mRNA compared with that of normal fibroblasts. In spite of this, we observed less response of the extrinsic fibroblasts to IL-1β stimulation in terms of MMP-13 mRNA than in normal tendon fibroblasts.

An anti-IL-1β strategy has attracted interest as a clinical treatment for inflammatory diseases such as a rheumatoid arthritis.[32] The findings of our study indicate that IL-1β is significantly involved in the remodelling of the grafted tendon after reconstruction of the ligament. Inhibition of IL-1β may prevent degradation of the graft and our study highlights a possible application of anti-IL-1β strategy for reducing the mechanical deterioration of grafted tendons after ligament reconstruction.

No benefits in any form have been received or will be received from a commercial party related directly or indirectly to the subject of this article.

## References


1. **Arnoczky SP, Tarvin GB, Marshall JL.** Anterior cruciate ligament replacement using patellar tendon: an evaluation of graft revascularization in the dog. *J Bone Joint Surg [Am]* 1982;64-A:217-24.
2. **Kleiner JB, Amiel D, Roux RD, Akeson WH.** Origin of replacement cells for the anterior cruciate ligament autograft. *J Orthop Res* 1986;4:466-74.
3. **Amiel D, Kleiner JB, Akeson WH.** The natural history of the anterior cruciate ligament autograft of patellar tendon origin. *Am J Sports Med* 1986;14:449-62.
4. **Hsu C, Chang J.** Clinical implications of growth factors in flexor tendon wound healing. *J Hand Surg [Am]* 2004;29:551-63.
5. **Marui T, Niyibizi C, Georgescu HI, et al.** Effect of growth factors on matrix synthesis by ligament fibroblasts. *J Orthop Res* 1997;15:18-23.
6. **Chang YC, Yang SF, Lai CC, Liu JY, Hsieh YS.** Regulations of matrix metalloproteinase production by cytokines, pharmacological agents and periodontal pathogens in human peridontal ligament fibroblasts cultures. *J Peridontal Res* 2002;37:196-203.
7. **Ikema Y, Tohyama H, Nakamura H, Kanaya F, Yasuda K.** Growth kinetics and integrin expression of fibroblasts infiltrating devitalised patellar tendons are different from those of intrinsic fibroblasts. *J Bone Joint Surg [Br]* 2005;87-B:1689-93.
8. **Tohyama H, Yasuda K, Uchida H.** Is the increase in type III collagen of the patellar tendon graft after ligament reconstruction really caused by "ligamentization" of the graft? *Knee Surg Sports Traumatol Arthrosc* 2006;14:1270-77.
9. **Knauper V, Will H, Lopez-Otin C, et al.** Cellular mechanisms for human procollagenase-3 (MMP-13) activation: evidence that MT1-MMP (MMP-14) and gelatinase a (MMP-2) are able to generate active enzyme. *J Biol Chem* 1996;271:17124-31.
10. **Freije JM, Diez-Itza I, Balbin M, et al.** Molecular cloning and expression of collagenase-3, a novel human matrix metalloproteinase produced by breast carcinomas. *J Biol Chem* 1994;269:16766-73.
11. **Mauviel A.** Cytokine regulation of metalloproteinase gene expression. *J Cell Biochem* 1993;53:288-95.
12. **Cao Q, Mak KM, Lieber CS.** Dilinoleoylphosphatidylcholine prevents transforming growth factor-beta1-mediated collagen accumulation in cultured rat hepatic stellate cells. *J Lab Clin Med* 2003;139:202-10.
13. **Tsuzaki M, Guyton G, Garrett W, et al.** IL-1 beta induces COX2, MMP-1, -3 and -13, ADAMTS-4, IL-1 beta and IL-6 in human tendon cells. *J Orthop Res* 2003;21:256-64.
14. **Arakawa M, Hatamochi A, Mori Y, et al.** Reduced collagenase gene expression in fibroblasts from hypertrophic scar tissue. *Br J Dermatol* 1996;134:863-8.
15. **Dasu MR, Hawkins HK, Barrow RE, Xue H, Herndon DN.** Gene expression profiles from hypertrophic scar fibroblasts before and after IL-6 stimulation. *J Pathol* 2004;202:476-85.
16. **Blaine TA, Kim YS, Voloshin I, et al.** The molecular pathophysiology of subacromial bursitis in rotator cuff disease. *J Shoulder Elbow Surg* 2005;14(Suppl 1):84-9.
17. **Gotoh M, Hamada K, Yamakawa H, et al.** Significance of granulation tissue in torn supraspinatus insertions: an immunohistochemical study with antibodies against interleukin-1 beta, cathepsin D, and matric metalloprotease-1. *J Orthop Res* 1997;15:33-9.

18. **Gotoh M, Hamada K, Yamakawa H, et al.** Perforation of rotator cuff increases interleukin 1beta production in the synovium of glenohumeral joint in rotator cuff diseases. *J Rheumatol* 2000;27:2886-92.
19. **Sakai H, Fujita K, Sakai Y, Mizuno K.** Immunolocalization of cytokines and growth factors in subacromial bursa of rotator cuff tear patients. *Kobe J Med Sci* 2001;47:25-34.
20. **Fahey TJ 3rd, Sherry B, Tracey KJ, et al.** Cytokine production in a model of wound healing: the appearance of MIP-1, MIP-2, cachectin/TNF and IL-1. *Cytokine* 1990;2:92-9.
21. **Grellner W, Georg T, Wilske J.** Quantitative analysis of proinflammatory cytokines (IL-1beta, IL-6, TNF-alpha) in human skin wounds. *Forensic Sci Int* 2000;113:251-64.
22. **Kondo T, Ohshima T.** The dynamics of inflammatory cytokines in the healing process of mouse skin wound: a preliminary study for possible wound age determination. *Int J Legal Med* 1996;108:231-6.
23. **Neta R, Oppenheim JJ.** Why should internists be interested in interleukin-1? *Ann Intern Med* 1988;109:1-3.
24. **Dinarello CA.** Biologic basis for interleukin-1 in disease. *Blood* 1996;87:2095-147.
25. **Nagineni CN, Amiel D, Green MH, Berchuck M, Akeson WH.** Characterization of the intrinsic properties of the anterior cruciate and medial collateral ligament cells: an in vitro cell culture study. *J Orthop Res* 1992;10:465-75.
26. **Hannafin JA, Attia ET, Warren RF, Bhargava MM.** Characterization of chemotactic migration and growth kinetics of canine knee ligament fibroblasts. *J Orthop Res* 1999;17:398-404.
27. **Archambault J, Tsuzaki M, Herzog W, Banes AJ.** Stretch and interleukin-1beta induce matrix metalloproteinase in rabbit tendon cells in vitro. *J Orthop Res* 2002;20:36-9.
28. **Chan BP, Chan KM, Maffulli N, Webb S, Lee KK.** Effect of basic fibroblast growth factor: an in vitro study of tendon healing. *Clin Orthop* 1997;342:239-47.
29. **Sadeghi M, Daniel V, Naujokat C, Weimer R, Opelz G.** Strikingly higher interleukin (IL)-1alpha, IL-1beta and soluble interleukin-1 receptor antagonist (sIL-1RA) but similar IL-2, IL-3, IL-4, IL-6, sIL-6R, IL-10, tumour necrosis factor (TNF)-alpha, transforming growth factor (TGF)-beta and interferon IFN-gamma urine levels in healthy females compared to healthy males: protection against urinary tract injury? *Clin Exp Immunol* 2005;142:312-17.
30. **Kropf J, Schurek JO, Wollner A, Gressner AM.** Immunological measurement of transforming growth factor-beta 1 (TGF-beta1) in blood: assay development and comparison. *Clin Chem* 1997;43:1965-74.
31. **Eppley BL, Woodell JE, Higgins J.** Platelet quantification and growth factor analysis from platelet-rich plasma: implications for wound healing. *Plast Reconstr Surg* 2004;114:1502-8.
32. **Afeltra A.** Treatment of rheumatoid arthritis: new therapeutic approaches with biological agents. *Curr Drug Targets Immune Endocr Metabol Disord* 2001;1:45-65.

Vaccine (2008) 26, 829–836

available at www.sciencedirect.com

ScienceDirect

journal homepage: www.elsevier.com/locate/vaccine

# Active immunization against macrophage migration inhibitory factor using a novel DNA vaccine prevents ovariectomy-induced bone loss in mice☆

Shin Onodera[a,*], Shigeki Oshima[b], Jun Nishihira[c], Kazunori Yasuda[a], Harukazu Tohyama[a], Kazuharu Irie[d], Yoshikazu Koyama[e]

[a] *Department of Sports Medicine and Joint Reconstruction Surgery, Hokkaido University Graduate School of Medicine, Kita-15, Nishi-7, Kita-ku, Sapporo, Hokkaido 060-8638, Japan*
[b] *Department of Orthopaedics, Hokkaido University Graduate School of Medicine, Kita-15, Nishi-7, Kita-ku, Sapporo, Hokkaido 060-8638, Japan*
[c] *Hokkaido Information University, 59-2 Nishi-Nopporo, Ebetsu, Hokkaido 069-8585, Japan*
[d] *Department of Oral Anatomy, Health Sciences University of Hokkaido School of Dentistry, 1757 Kanazawa, Tobetsu-cho, Ishikari-gun, Hokkaido 061-0293, Japan*
[e] *Department of Biochemistry, Hokkaido University Graduate School of Medicine, Kita-15, Nishi-7, Kita-ku, Sapporo, Hokkaido 060-8638, Japan*

Received 4 April 2007; received in revised form 31 October 2007; accepted 22 November 2007
Available online 17 December 2007

**KEYWORDS**
Macrophage migration inhibitory factor;
Ovariectomy;
Vaccine

**Summary** Previous studies have demonstrated that mice deficient in the macrophage migration inhibitory factor (MIF) gene are protected from ovariectomy (OVX)-induced bone loss. We developed a novel MIF-deoxyribonucleic acid (DNA) vaccine by introducing oligonucleotides encoding a helper T epitope into the cDNA sequence of murine MIF. Mice given the MIF-DNA vaccine produced high titers of autoantibody against MIF, and were protected from OVX-induced bone loss. Our results further support the hypothesis that MIF is involved in the pathomechanism of OVX-induced bone loss, and also show that active immunization against MIF using a DNA vaccine may be useful for the prophylactic treatment of postmenopausal osteoporosis.


## Introduction

Postmenopausal osteoporosis is one of the major health problems that affect elderly women in developed countries. Estrogen deficiency increases bone turnover, which leads to enhanced bone resorption and an increased risk of fracture [1]. There is now a large body of evidence suggesting that estrogen deficiency after natural or surgically induced

☆ This work was supported in part by a Grant-in-Aid from the Ministry of Science and Education of Japan (17591542).
* Corresponding author. Tel.: +81 11 706 7211; fax: +81 11 706 7822.
*E-mail address:* onodera@med.hokudai.ac.jp (S. Onodera).

0264-410X/$ – see front matter © 2007 Elsevier Ltd. All rights reserved.
doi:10.1016/j.vaccine.2007.11.066

menopause increases the production of proinflammatory cytokines such as interleukin (IL)-1, IL-6, and tumor necrosis factor (TNF)-α [2–5]. These proinflammatory cytokines appear to enhance osteoclast formation and to activate mature osteoclasts, which increases bone resorption [6,7]. In addition, animal models have shown that the deficiency or functional block of one of these cytokines can prevent the bone loss induced by ovariectomy (OVX) [8].

Macrophage Migration Inhibitory Factor (MIF) was initially identified as a soluble factor that was secreted into the culture medium by activated T cells [9,10]. After the MIF cDNA was cloned [11], the novel biological functions of MIF were reported. MIF is a proinflammatory cytokine and glucocorticoid-induced immunomodulator that is released in response to a variety of inflammatory stimuli [12–14]. An emerging body of data indicates that MIF acts within cytokine cascades to control the 'set point' and magnitude of the immune and inflammatory response [15]

The bone loss that follows estrogen deficiency may be because estrogen normally suppresses the production of inflammatory cytokines at the transcriptional level. Upon gonadal dysfunction such as menopause, this suppressive effect is lifted and the resulting enhanced production of inflammatory cytokines then leads to elevated bone resorption. Recently, a link between MIF and estrogen emerged. It was reported that MIF is up-regulated in the wound-healing process of estrogen-deficient mice, and that estrogen decreases MIF production by murine macrophages [16]. Moreover, estrogen suppresses the transcription of MIF [17]. These observations suggest that MIF may be involved in the pathomechanism of bone loss arising from estrogen deficiency. Indeed, it could be a key player in this mechanism since MIF is believed to be an upstream regulator that controls the production of inflammatory cytokines such as TNF-α and IL-1 that are considered to play pivotal roles in estrogen deficiency-induced bone loss. Supporting this notion is our recent study showing that mice deficient in the MIF gene (MIF KO) were protected from OVX-induced trabecular bone loss [18]. This observation strongly suggests that MIF is located well upstream in the inflammatory cytokine cascade that participates in OVX-induced bone loss.

Several approaches that aim to suppress the bioactivity of cytokines involved in bone resorption have been reported. The target cytokines for these experimental trials include IL-1, TNF-α, IL-6, and receptor activator of nuclear factor kappa-β ligand (RANKL) [19–22]. However, attempts to prevent OVX-induced bone loss by suppressing MIF bioactivity have not been reported. Recently, we developed a novel DNA vaccine that elicits an autoantibody against MIF and suppresses the incidence and severity of arthritis in two murine experimental models of arthritis [23]. The purpose of the study reported here was to investigate whether this novel approach targeting MIF could also be used to suppress OVX-induced bone loss.

## Materials and methods

### Animals

Female BALB/c mice (3 weeks old) were purchased from Sankyo Laboratory Service (Shizuoka, Japan). All mice were maintained under specific pathogen-free conditions. All animal procedures were conducted using a protocol that followed the guidelines and was approved by the Hokkaido University Institutional Animal Care and Use Committee. Bilateral OVX or sham surgeries were performed under anesthesia. Four weeks after surgery, all mice were sacrificed by means of an overdose of anesthesia.

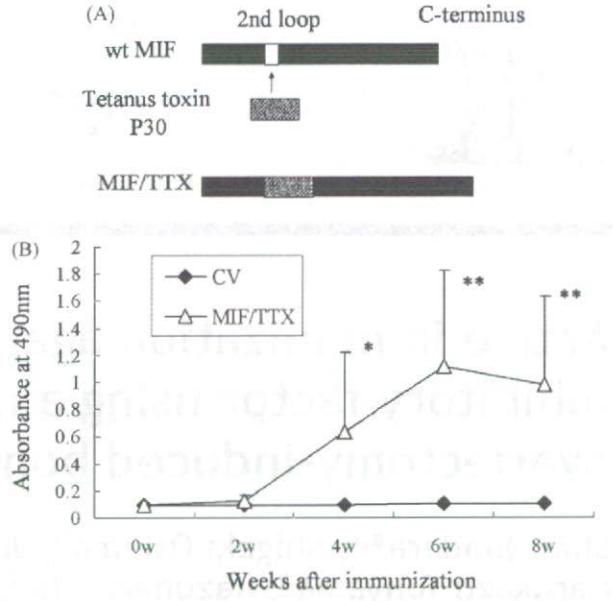


**Figure 1** (A) Design of a DNA construct that expresses a mMIF variant whose second loop bears a promiscuous $T_H$ epitope from TTX. To generate this construct, mMIF cDNA was cloned into the mammalian expression vector pCAGGS, after which the 2nd loop region of MIF cDNA was substituted with the $T_H$ epitope. (B) Immunization with the $T_H$-modified MIF-DNA vaccine elicits autoantibodies that cross-react with native mMIF. Anti-mMIF titers in sera from groups of 5 mice vaccinated with 25 μg of endotoxin-free pCAGGS (control vaccine [CV]) and MIF/TTX in 0.9% sterile saline. The results shown are means ± SD. $^{*}p < 0.005$, $^{**}p < 0.0001$ vs. CV at the same time-point.

### Construction of the MIF/TTX expression plasmid

murine MIF (mMIF) cDNA was cloned into the mammalian expression vector pCAGGS [24]. We sought to generate an immunologically active MIF antigen by replacing the second loop region of MIF with a TTX $T_H$ epitope. To do this, the cDNA region that encodes the second loop of mMIF (amino acids 32–37; GKPAQY) was deleted from the MIF cDNA and substituted with an EcoRI site by standard PCR-based techniques. cDNA encoding the TTX P30 $T_H$ epitope (FNNFTVSFWLRVPKVSASHL [25]) with an EcoRI site at both termini was obtained by hybridization of partially overlapping oligo DNAs (sense, ggaattcaacaacttcaccgtgagcttctggctgcgcgtgcccaa and anti-sense, ggaattccaggtggctggcgctcaccttgggcacgcgcagccaga) and subsequent polymerization with Klenow's DNA polymerase fragment. After digestion with EcoRI, the P30 cDNA was inserted into the EcoRI site of the MIF expression plasmid (Fig. 1A) and a clone bearing the

correctly oriented insert was selected. The MIF/TTX plasmid DNA was then purified by alkaline lysis followed by two rounds of CsCl density gradient ultracentrifugation. This preparation was used for animal vaccination.

### Intramuscular DNA injection and electroporation

Gene transfer into muscle by electroporation was performed essentially as described previously [26]. Four-week-old mice were anesthetized with ether and shaved around their hind legs, after which a pair of electrode needles (5 mm gap and 0.5 mm diameter, NEPA GENE, Chiba, Japan) was inserted into an anterior tibial muscle. The DNA vaccine (25 μg/25 μl, 0.9% saline) was then injected into the portion of the leg between the needles. This was followed by three electric pulses of 50 V and 50 msec that were applied by using an electric pulse generation system (T820 and Optimizer 500, BTX, San Diego, CA) and were followed by another three pulses with inverted polarity. The other tibial muscle was then also injected and electroporated. As a result, each mouse received 50 μg of the naked plasmid.

### Evaluation of anti-MIF Ab titers in the sera of DNA-vaccinated mice

Anti-MIF titers in the plasma were determined by a direct enzyme-linked immunosorbent assay (ELISA). Briefly, individual plasmas from vaccinated mice were collected from the tail vein and diluted with 0.1% bovine serum albumin/PBS/0.05% Tween 20. Small aliquots of 1:200 diluted plasma were placed in 96 well flat-bottom plates precoated with recombinant mMIF. The serum anti-MIF antibodies that reacted with the precoated MIF were detected by HRP-conjugated goat anti-mouse antibody and color development with a substrate reagent (Techne, Minneapolis, MN).

### Microcomputed Tomography (μCT)

The right femora of each animal was fixed in 10% formaldehyde after removing the soft tissues and analyzed by a μCT system (ScanXmate-A090S, Comscan Techno Corporation, Tokyo, Japan). The two-dimensional image of the trabecular bone was quantified as follows. Axial bone slices with a thickness of 8.76 μm were made in the area that is 10% proximal to the distal growth plate of the femora. The mean volume (bone volume/tissue volume; BV/TV), thickness (trabecular thickness; Tb.Th), and separation of the trabecular bone (trabecular separation; Tb.Sp) in the slices were quantified by an image analyzer (Luzex-F, Nireco, Tokyo, Japan).

### Histomorphometric analysis of bone

For histological analysis, serial 5 μm sections of proximal tibiae were made and stained with toluidine blue. For bone histomorphometric analysis, mice were injected subcutaneously with 8 mg/kg body weight of calcein 4 and 1 days before sacrifice. The right tibia of each mouse was then fixed with 70% ethanol, embedded in methyl methacrylate (MMA) without decalcification, and serially sectioned (5 μm) by using a microtome. The sections were then stained by Villanueva-Goldner's trichrome method, which discriminates between mineralized and unmineralized bone. The sections were also stained for identification of cellular components. The stained bone sections were analyzed by using an image analyzer (System Supply Co., Nagano, Japan). The measurements were performed in an area that was 1.2 mm in length and located 0.3 mm below the growth plate at the proximal metaphysis of the tibiae. Histomorphometry was conducted as previously defined [27]. The parameters that were measured were the bone volume per tissue volume (BV/TV, %), the trabecular thickness (Tb.Th, μm), the trabecular number (Tb.N, $mm^{-1}$), the trabecular separation (Tb.Sp, μm), the osteoid volume per bone volume (OV/BV, %), the osteoid surface per bone surface (OS/BS, %), the osteoblast surface per bone surface (Ob.S/BS, %), the eroded surface per bone surface (ES/BS, %), the number of osteoclasts per the bone perimeter (N.Oc/B.Pm, per 100 mm), the osteoclast surface per bone surface (Oc.S/BS, %), the mineral apposition rate (MAR, $day^{-1}$), the mineralized surface per bone surface (MS/BS, %), and the bone formation rate per bone surface (BFR/BS, $mm^3/cm^2/y$).

The data were evaluated for statistical significance by one-way ANOVA using Fisher's test as a post hoc test. A $p$ value of $< 0.05$ was considered to be statistically significant.

## Results

### BALB/c mice vaccinated with MIF/TTX generate anti-MIF Abs

As shown in Fig. 1A, we generated a DNA vaccine that expresses a mMIF variant whose second loop bears a promiscuous $T_H$ epitope from TTX. Initially, we tested whether this DNA vaccine could induce a polyclonal antibody response that recognized native MIF. Thus, both tibial muscles of BALB/c mice (five mice per group) were each vaccinated once intramuscularly with 25 μg of MIF/TTX or control vector (CV) DNA in 0.9% saline by electroporation. Thus, each mouse received 50 μg of vaccine. Four weeks after vaccination, the MIF/TTX-vaccinated mice had autoantibodies that reacted to native MIF (Fig. 1B) whereas the CV failed to raise such MIF-reactive antibodies. These differences were statistically significant (MIF/TTX vs. pCAGGS: $p < 0.005$ at 4 weeks, and $p < 0.0001$ at 6 and 8 weeks). Thus, incorporating the TTX $T_H$ epitope bypasses the immunological tolerance of mice to the MIF self-protein.

### Trabecular bone loss in the distal femur

We then injected groups of 22 BALB/c mice with MIF/TTX and 21 BALB/c mice with CV DNA, and 4 weeks later subjected them to bilateral OVX or sham surgery. Four weeks later, all mice were sacrificed and their distal trabecular femoral bones were examined by μCT for an OVX-associated reduction in volume (BV/TV), thickness, and separation of trabecular bone, as follows. This analysis revealed that OVX had similar effects on CV-administered mice as on normal female BALB/c mice, as shown by our previous study [18]. In other words, the femoral bones of OVX CV mice showed a significant decrease in trabecular bone compared to sham-operated CV mice (Fig. 2A, B). In contrast, the bones of

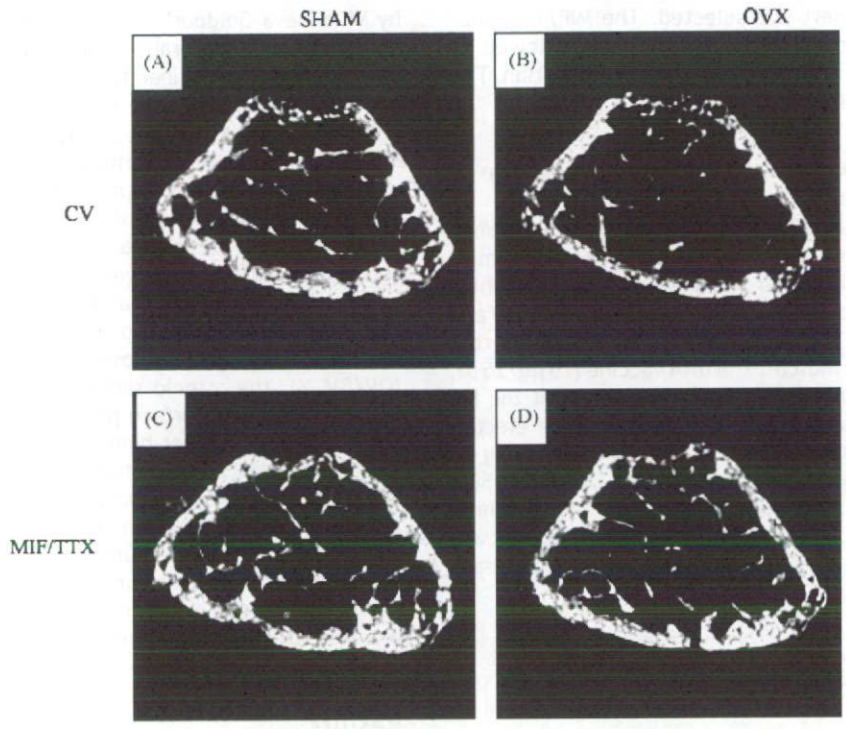


**Figure 2** μCT analysis of the right femora of mice 4 weeks after OVX or sham operation. (A) CV-vaccinated and sham-operated mice. (B) CV-vaccinated and ovariectomized mice. (C) MIF/TTX-vaccinated and sham-operated mice. (D) MIF/TTX-vaccinated and ovariectomized mice. Axial femur bone slices were made as described in the "Materials and Methods". The slices that are 10% proximal to the distal growth plate of the femora are shown.

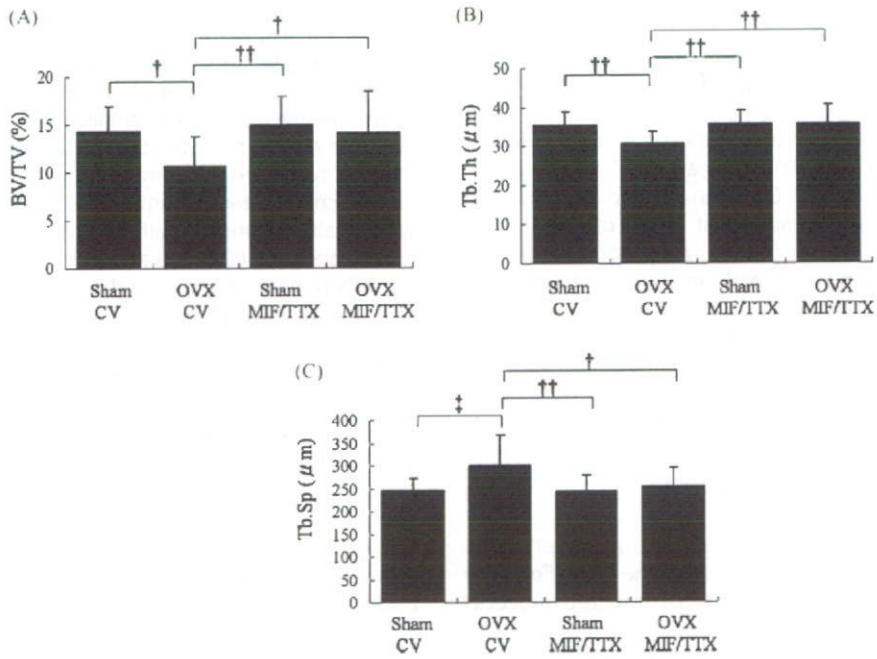


**Figure 3** Quantification of the two-dimensional μCT-based values. (A-C) MIF/TTX-vaccinated mice were protected from the OVX-induced reductions in BV/TV (A), decreases in trabecular thickness (B), and increases in trabecular separation (C) that were observed in CV-vaccinated mice. The values shown are means ± SD. $n = 10–11$ in all groups; $^{\dagger}p < 0.05$, $^{\ddagger}p < 0.01$, $^{\dagger\dagger}p < 0.005$ vs. OVX CV animals.

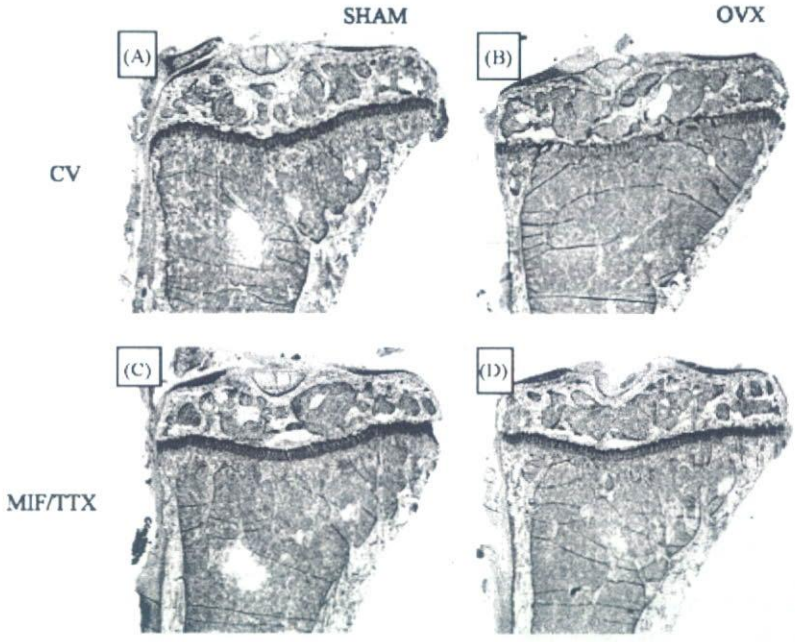


**Figure 4** Toluidine blue staining of the tibiae of mice 4 weeks after OVX or sham operation. (A) CV-vaccinated and sham-operated mice. (B) CV-vaccinated and ovariectomized mice. (C) MIF/TTX-vaccinated and sham-operated mice. (D) MIF/TTX-vaccinated and ovariectomized mice.

MIF/TTX-administered mice were unchanged by OVX (Fig. 2C and D). When the two-dimensional μCT-based values were quantified, the BV/TV values of the sham-operated CV- and MIF/TTX-administered mice were similar. Relative to these values, OVX significantly reduced the BV/TV of CV-administered mice ($p < 0.05$, Fig. 3A). The OVX CV- and MIF/TTX-administered mice showed a significant difference in their BV/TV ($p < 0.05$, Fig. 3A). Compared with sham-operated CV-administered mice, OVX also decreased the trabecular thickness ($p < 0.005$, Fig. 3B) and increased the trabecular separation ($p < 0.01$, Fig. 3C) in CV-administered mice. However, the MIF/TTX vaccine protected the mice from these OVX-associated changes (Fig. 3).

## Bone histomorphometry in OVX CV- or MIF/TTX-treated mice

Histological observation revealed that, relative to sham-operated animals, OVX reduced the cancellous bone volume

**Table 1** Proximal tibial bone histomorphometric dynamic parameters in CV- and MIF/TTX-treated mice with or without OVX

| Bone parameters | CV-Sham | CV-OVX | MIF/TTX-Sham | MIF/TTX-OVX |
|---|---|---|---|---|
| Static parameters | | | | |
| BV/TV (%) | 6.30 ± 1.26 | 4.14 ± 1.55 | 6.45 ± 1.87 | 5.99 ± 2.40 |
| Tb.Th (μm) | 28.3 ± 1.46 | 26.7 ± 4.16 | 30.7 ± 5.09 | 29.1 ± 5.01 |
| Tb.N ($mm^{-1}$) | 2.22 ± 0.38[a] | 1.54 ± 0.56 | 2.07 ± 0.38 | 1.95 ± 0.36 |
| Tb.Sp (μm) | 433 ± 73.1[a] | 724 ± 358 | 466 ± 93.7 | 499 ± 105 |
| Formation parameters | | | | |
| OV/BV (%) | 0.43 ± 0.30[b] | 2.04 ± 1.55 | 0.59 ± 0.57[a] | 0.68 ± 0.18[a] |
| OS/BS (%) | 5.00 ± 2.19[a] | 10.8 ± 6.53 | 4.85 ± 2.67[a] | 5.16 ± 1.49[a] |
| Ob.S/BS (%) | 12.9 ± 5.47 | 19.7 ± 7.97 | 10.7 ± 2.74[a] | 11.4 ± 2.48[a] |
| Resorption parameters | | | | |
| ES/BS (μm) | 2.80 ± 1.38 | 3.77 ± 1.78 | 2.45 ± 1.09 | 2.77 ± 1.21 |
| N.Oc/B.Pm (per 100 mm) | 244 ± 86.2[a] | 336 ± 62.9 | 181 ± 28.1[d] | 182 ± 34.0[d] |
| Oc.S/BS (%) | 2.68 ± 1.08[e] | 5.68 ± 1.48 | 2.14 ± 0.44[e] | 1.87 ± 0.39[e] |
| MAR ($day^{-1}$) | 1.17 ± 0.42[a] | 1.75 ± 0.45 | 1.01 ± 0.19[c] | 1.09 ± 0.15[b] |
| MS/BS (%) | 14.1 ± 3.59 | 15.5 ± 2.12 | 12.9 ± 3.50 | 17.7 ± 2.35[f] |
| BFR/BS ($mm^3/cm^2/y$) | 2.67 ± 1.52 | 3.60 ± 1.87 | 1.51 ± 0.71[a] | 2.70 ± 1.74[b] |

Values are shown as mean ± SD ($n = 5$ per group) vs. CV-OVX; [a]$p < 0.05$, [b]$p < 0.01$, [c]$p < 0.005$, [d]$p < 0.001$, [e]$p \leq 0.0001$. vs. MIF/TTX-Sham; [f]$p < 0.05$.

in the proximal region of the tibiae in CV-administered mice (Fig. 4A and B) but not in MIF/TTX-administered mice (Fig. 4C and D). These bone dynamics were confirmed by bone histomorphometry (Table 1), which showed that in CV-administered mice, OVX elevated the bone formation parameters OV/BV and OS/BS ($p < 0.01$ and $p < 0.05$, respectively) and the bone resorption parameters N.Oc/B.Pm and Oc.S/BS ($p < 0.05$ and $p = 0.0001$, respectively), similar to what we have observed in normal female BALB/c mice [18]. However, the MIF/TTX-administered mice were resistant to these effects of OVX and showed significantly lower OV/BV, OS/BS, Ob.S/BS, N.Oc/B.Pm and Oc.S/BS values after OVX than CV-administered mice ($p < 0.05$, $p < 0.05$, $p < 0.05$, $p < 0.001$, and $p < 0.0001$, respectively).

## Discussion

In this study, we demonstrated that OVX-induced bone loss can be effectively suppressed by our novel approach, i.e., active immunization against MIF using a DNA vaccine. It is widely accepted that after menopause, the depletion of estrogen causes high bone turnover that changes the bone metabolic balance to one dominated by resorption, which results in osteoporosis [28,29]. Indeed, our histomorphometric analyses of the tibiae of CV-administered mice revealed that their OVX-induced bone loss was associated with increased osteoclastic bone resorption. In contrast, the resistance of MIF/TTX-administered mice to bone loss after OVX was associated with lower levels of osteoclastic bone resorption (N.Oc/B.Pm and Oc.S/BS) values.

Estrogen deficiency after OVX causes the enhanced production of bone-resorbing cytokines such as IL-1 and TNF-α by circulating monocytes [4–7]. Although circulating levels of MIF are also rapidly enhanced by OVX, our recent study suggests that MIF does not directly up-regulate RANKL mRNA expression or induce osteoclastogenesis [30]. Instead, as suggested by several lines of evidence, it seems that MIF is located upstream of these bone-resorbing cytokines, where it regulates their production. Indeed, *in vitro* and *in vivo* studies have shown that MIF can induce and regulate the production of TNF and IL-1 [14,31–34]. An emerging body of data now indicates that MIF acts within the cytokine cascade to control the 'set point' and magnitude of the immune and inflammatory response [15]. Therefore, we speculate that the enhanced production of bone-resorbing cytokines after OVX is due, at least in part, to the rapid increase in serum MIF. While the types of cells that produce MIF after OVX have not yet been clearly identified, it is possible that they may include T cells, whose involvement in the pathomechanism of OVX-induced bone loss has been elucidated recently. Weitsmann et al. have proposed that the enhancement of T cell-derived TNF-α levels following OVX is the key to OVX-induced bone loss, and that IL-7 plays a pivotal role in this event as an upstream regulator of TNF [35,36]. It is possible that MIF, which was originally identified as a T cell-derived cytokine, plays an important role in the intercellular events that take place and include T cells after OVX. It is also possible that IL-7 and MIF may interact in some way, and that this interaction is activated by OVX. Further investigations are necessary to test these possibilities.

Currently marketed osteoporosis therapies, which include the use of bisphosphonates and selective estrogen modulators, are efficacious but inconvenient for the patient because they must be administered frequently. Each drug is also associated with a risk of adverse side effects. To suppress the cytokines involved in OVX-induced bone loss, several anti-cytokine approaches using recombinant proteins such as IL-1Ra, soluble TNF receptor, and osteoprotegerin (OPG) (a soluble decoy receptor of RANKL) have been tested [19,20,22]. Indeed, a genetically engineered OPG-Fc fusion protein has already been subjected to clinical trials and has proven efficient in reducing bone turnover in postmenopausal women [37]. However, the routine use of OPG is limited by its high cost and the expected need to frequently administer the drug. Several trials seeking to suppress the bioactivities of the bone loss-inducing cytokines by injecting neutralizing antibodies have also been reported. In the murine OVX model, administration of anti-IL-6 antibody did not prevent OVX-induced bone loss, although the anti-IL-11 antibody was effective [21,38]. However, these passive immunization therapies are not only hampered by high costs, but it remains possible that these molecules can also induce immunogenic antibody–antibody responses that could limit the long-term efficacy of these treatments. This latter problem may be overcome by actively inducing specific antibodies in the host against the target cytokine. Indeed, this approach has been utilized in experimental trials aiming to raise antibodies against RANKL [39,40]. The MIF-DNA vaccine we used in this study, which was originally developed to suppress inflammatory diseases, has previously exhibited a siginificant prophylactic effect against experimental arthritis [23]. We hypothesized that this vaccine could also be used to suppress OVX-induced bone loss on the basis of two experimental findings. First, the MIF-DNA vaccine efficiently elicits autoantibodies that react to MIF [23], and second, mice that lack the MIF gene are protected against OVX-induced bone loss [18]. Indeed, we showed in this study that blocking MIF promotes resistance to OVX-induced bone loss, which is additional evidence that this cytokine plays an important role in the pathomechanism of OVX-induced bone loss. However, it remains unclear whether MIF, relative to other cytokines, is indeed superior as the target molecule for the treatment of postmenopausal osteoporosis. This question can only be answered when we understand in more detail how MIF is involved in OVX-induced bone loss.

Concerning the predicted problems that might arise from continuous suppression of MIF bioactivity, it should be noted that the presence of autoantibody against cytokines is not necessarily harmful. Indeed, it could be protective against diseases, as exemplified by the finding of Jouvenne et al., who reported that the titer of autoantibodies to IL-1α correlated negatively with the disease severity of chronic arthritis [41]. Moreover, previous reports of active immunization against cytokines have revealed that the autoantibody titer tends to gradually decrease over time. Thus, it is unlikely that a single administration of such a vaccine is irreversible [42]. Rather, to acquire and maintain high autoantibody titers, it may be necessary to provide booster injections or re-vaccination [43]. Notably, we did not detect elevated mortality or delayed wound healing in mice given the MIF-TTX DNA vaccine (unpublished observations), though further

detailed investigations are necessary to confirm these observations.

In summary, in this study we provided further evidence of the pivotal role MIF plays in the pathogenesis of estrogen deficiency-induced bone loss. We also presented a novel therapeutic approach for this disease. Our observations suggest that MIF may be a candidate target for a novel osteoporosis therapeutic approach.

## Acknowledgements

We are grateful to Chiyo Imaizumi of Hokkaido University Graduate School of Medicine, Department of Sports Medicine and Joint Reconstruction Surgery, for technical assistance. We are also grateful to Ayako Shiraishi of Chugai Co. Ltd. for technical assistance. This work was supported by a Grant-in-Aid from the Ministry of Science and Education of Japan (17591542).

## References

[1] NIH Consensus Development Panel on Osteoporosis Prevention, Diagnosis, and Therapy. Osteoporosis prevention, diagnosis, and therapy. JAMA 2001;285(6):785–95.
[2] Manolagas SC, Kousteni S, Jilka RL. Sex steroids and bone. Recent Prog Horm Res 2002;57:385–409.
[3] Rogers A, Eastell R. The effect of 17beta-estradiol on production of cytokines in cultures of peripheral blood. Bone 2001;29(1):30–4.
[4] Pfeilschifter J, Koditz R, Pfohl M, Schatz H. Changes in proinflammatory cytokine activity after menopause. Endocr Rev 2002;23(1):90–119.
[5] Pacifici R. Estrogen, cytokines, and pathogenesis of postmenopausal osteoporosis. J Bone Miner Res 1996;11 (8):1043–51.
[6] Van Bezooijen RL, Farih-Sips HC, Papapoulos SE, Lowik CW. IL-1alpha, IL-1beta, IL-6, and TNF-alpha steady-state mRNA levels analyzed by reverse transcription-competitive PCR in bone marrow of gonadectomized mice. J Bone Miner Res 1998;13(2):185–94.
[7] Jilka RL, Hangoc G, Girasole G, Passeri G, Williams DC, Abrams JS, et al. Increased osteoclast development after estrogen loss: mediation by interleukin-6. Science 1992;257(5066):88–91.
[8] Teitelbaum SL. Postmenopausal osteoporosis, T cells, and immune dysfunction. Proc Natl Acad Sci USA 2004; 101(48):16711–2.
[9] Bloom BR, Bennett B. Mechanism of a reaction in vitro associated with delayed-type hypersensitivity. Science 1966; 153(731):80–2.
[10] David JR. Delayed hypersensitivity in vitro: its mediation by cell-free substances formed by lymphoid cell-antigen interaction. Proc Natl Acad Sci USA 1966;56(1):72–7.
[11] Weiser WY, Temple PA, Witek-Giannotti JS, Remold HG, Clark SC, David JR. Molecular cloning of a cDNA encoding a human macrophage migration inhibitory factor. Proc Natl Acad Sci USA 1989;86(19):7522–6.
[12] Bernhagen J, Calandra T, Mitchell RA, Martin SB, Tracey KJ, Voelter W, et al. MIF is a pituitary-derived cytokine that potentiates lethal endotoxaemia. Nature 1993;365(6448):756–9.
[13] Nishino T, Bernhagen J, Shiiki H, Calandra T, Dohi K, Bucala R. Localization of macrophage migration inhibitory factor (MIF) to secretory glanules within the corticotrophic and thyrotrophic cells of the pituitary gland. Mol Med 1995;1(7):781–8.
[14] Calandra T, Bernhagen J, Mitchell RA, Bucala R. The macrophage is an important and previously unrecognized source of macrophage migration inhibitory factor. J Exp Med 1994;179(6):1895–902.
[15] Baugh JA, Donnelly SC. Macrophage migration inhibitory factor: a neuroendocrine modulator of chronic inflammation. J Endocrinol 2003;179(1):15–23.
[16] Ashcroft GS, Mills SJ, Lei K, Gibbons L, Jeong MJ, Taniguchi M, et al. Estrogen modulates cutaneous wound healing by down-regulating macrophage migration inhibitory factor. J Clin Invest 2003;111(9):1309–18.
[17] Hardman MJ, Waite A, Zeef L, Burow M, Nakayama T, Ashcroft GS. Macrophage migration inhibitory factor: a central regulator of wound healing. Am J Pathol 2005;167(6):1561–74.
[18] Oshima S, Onodera S, Amizuka N, Li M, Irie K, Watanabe S, et al. Macrophage migration inhibitory factor-deficient mice are resistant to ovariectomy-induced bone loss. FEBS Lett 2006;580(5):1251–6.
[19] Kitazawa R, Kimble RB, Vannice JL, Kung VT, Pacifici R. Interleukin-1 receptor antagonist and tumor necrosis factor binding protein decrease osteoclast formation and bone resorption in ovariectomized mice. J Clin Invest 1994; 94(6):2397–406.
[20] Kimble RB, Matayoshi AB, Vannice JL, Kung VT, Williams C, Pacifici R. Simultaneous block of interleukin-1 and tumor necrosis factor is required to completely prevent bone loss in the early postovariectomy period. Endocrinology 1995;136(7):3054–61.
[21] Kimble RB, Bain S, Pacifici R. The functional block of TNF but not of IL-6 prevents bone loss in ovariectomized mice. J Bone Miner Res 1997;12(6):935–41.
[22] Simonet WS, Lacey DL, Dunstan CR, Kelley M, Chang MS, Luthy R, et al. Osteoprotegerin: a novel secreted protein involved in the regulation of bone density. Cell 1997;89(2):309–19.
[23] Onodera S, Ohshima S, Tohyama H, Yasuda K, Nishihira J, Iwakura Y, et al. A novel DNA vaccine targeting macrophage migration inhibitory factor protects joints from inflammation and destruction in murine models of arthritis. Arthritis Rheum 2007;56(2):521–30.
[24] Niwa H, Yamamura K, Miyazaki J. Efficient selection for high-expression transfectants with a novel eukaryotic vector. Gene 1991;108(2):193–9.
[25] Panina-Bordignon P, Tan A, Termijtelen A, Demotz S, Corradin G, Lanzavecchia A. Universally immunogenic T cell epitopes: promiscuous binding to human MHC class II and promiscuous recognition by T cells. Eur J Immunol 1989;19(12):2237–42.
[26] Aihara H, Miyazaki J. Gene transfer into muscle by electroporation in vivo. Nat Biotech 1998;16(9):867–70.
[27] Parfitt AM, Drezner MK, Glorieux FH, Kanis JA, Malluche H, Meunier PJ, et al. Bone histomorphometry: standardization of nomenclature, symbols, and units Report of the ASBMR Histomorphometry Nomenclature Committee. J Bone Miner Res 1987;2(6):595–610.
[28] Riggs BL, Khosla S, Atkinson EJ, Dunstan CR, Melton LJ 3rd Evidence that type I osteoporosis results from enhanced responsiveness of bone to estrogen deficiency. Osteoporosis Int 2003;14(9):728–33.
[29] Lindsay R. Prevention and treatment of osteoporosis. Lancet 1993;341(8848):801–5.
[30] Onodera S, Sasaki S, Ohshima S, Amizuka N, Li M, Udagawa N, et al. Transgenic mice overexpressing macrophage migration inhibitory factor (MIF) exhibit high-turnover osteoporosis. J Bone Miner Res 2006;21(6):876–85.
[31] Bernhagen J, Mitchell RA, Calandra T, Voelter W, Cerami A, Bucala R. Purification, bioactivity, and secondary structure analysis of mouse and human macrophage migration inhibitory factor (MIF). Biochemistry 1994;33(47):14144–55.
[32] Morand EF, Leech M. Macrophage migration inhibitory factor in rheumatoid arthritis. Front Biosci 2005;10:12–22.
[33] Leech M, Metz C, Hall P, Hutchinson P, Gianis K, Smith M, et al. Macrophage migration inhibitory factor in rheumatoid arthri-

tis: evidence of proinflammatory function and regulation by glucocorticoids. Arthritis Rheum 1999;42(8):1601–8.
[34] Morand EF, Bucala R, Leech M. Macrophage migration inhibitory factor: an emerging therapeutic target in rheumatoid arthritis. Arthritis Rheum 2003;48(2):291–9.
[35] Weitzmann MN, Roggia C, Toraldo G, Weitzmann L, Pacifici R. Increased production of IL-7 uncouples bone formation from bone resorption during estrogen deficiency. J Clin Invest 2002;110(11):1643–50.
[36] Toraldo G, Roggia C, Qian WP, Pacifici R, Weitzmann MN. IL-7 induces bone loss in vivo by induction of receptor activator of nuclear factor kappa B ligand and tumor necrosis factor alpha from T cells. Proc Natl Acad Sci USA 2003;100(1):125–30.
[37] Bekker PJ, Holloway D, Nakanishi A, Arrighi M, Leese PT, Dunstan CR. The effect of a single dose of osteoprotegerin in postmenopausal women. J Bone Miner Res 2001;16(2):348–60.
[38] Shaughnessy SG, Walton KJ, Deschamps P, Butcher M, Beaudin SM. Neutralization of interleukin-11 activity decreases osteoclast formation and increases cancellous bone volume in ovariectomized mice. Cytokine 2002;20(2):78–85.
[39] Juji T, Hertz M, Aoki K, Horie D, Ohya K, Gautam A, et al. A novel therapeutic vaccine approach, targeting RANKL, prevents bone destruction in bone-related disorders. J Bone Miner Metab 2002;20(5):266–8.
[40] Spohn G, Schwarz K, Maurer P, Illges H, Rajasekaran N, Choi Y, et al. Protection against osteoporosis by active immunization with TRANCE/RANKL displayed on virus-like particles. J Immunol 2005;175(9):6211–8.
[41] Jouvenne P, Fossiez F, Banchereau J, Miossec P. High levels of neutralizing autoantibodies against IL-1 alpha are associated with a better prognosis in chronic polyarthritis: a follow-up study. Scand J Immunol 1997;46(4):413–8.
[42] Dalum I, Butler DM, Jensen MR, Hindersson P, Steinaa L, Waterston AM, et al. Therapeutic antibodies elicited by immunization against TNF-alpha. Nat Biotechnol 1999;17(7):666–9.
[43] Zagury D, Le Buanec H, Bizzini B, Burny A, Lewis G, Gallo RC. Active versus passive anti-cytokine antibody therapy against cytokine-associated chronic diseases. Cytokine Growth Factor Rev 2003;14(2):123–37.

# Fracture of Ni-Ti superelastic alloy under sustained tensile load in physiological saline solution containing hydrogen peroxide

**Ken'ichi Yokoyama,[1] Toshio Ogawa,[2] Atsushi Fujita,[2] Kenzo Asaoka,[1] Jun'ichi Sakai[2]**
[1]*Department of Biomaterials and Bioengineering, Institute of Health Biosciences, The University of Tokushima Graduate School, 3-18-15 Kuramoto-cho, Tokushima 770-8504, Japan*
[2]*Department of Materials Science and Engineering, Waseda University, 3-4-1 Okubo, Shinjuku-ku, Tokyo 169-8555, Japan*

Received 2 June 2006; revised 9 August 2006; accepted 3 November 2006
Published online 20 February 2007 in Wiley InterScience (www.interscience.wiley.com). DOI: 10.1002/jbm.a.31173

**Abstract:** The fracture of Ni-Ti superelastic alloy has been investigated by a sustained tensile-loading test in physiological saline solution containing hydrogen peroxide (0.15*M* NaCl + 0.3*M* $H_2O_2$). The fracture always occurs when the applied stress exceeds the critical stress for martensite transformation. In contrast, under a low applied stress, the fracture does not always occur within 1000 h. The fracture is probably mainly caused by localized corrosion associated with the preferential dissolution of nickel ions. In 0.3*M* $H_2O_2$ solution without NaCl, the fracture does not occur even under a high applied stress. The results of the present study imply that one reason for the fracture of the Ni-Ti superelastic alloy *in vivo* is localized corrosion due to the synergistic effects of hydrogen peroxide and sodium chloride under applied stress. © 2007 Wiley Periodicals, Inc. J Biomed Mater Res 82A: 558–567, 2007

**Key words:** Ni-Ti; fracture; corrosion; hydrogen peroxide

## INTRODUCTION

Ni-Ti superelastic alloy is widely used in biomedical applications and is a promising new implant material,[1–4] not only because of its unique superelastic property but also its good ductility, fatigue life, and wear resistance.[5] Furthermore, the alloy exhibits good corrosion resistance *in vitro*, such as in physiological saline and simulated body fluids.[6–11] *In vivo*, however, the fracture of devices made of the alloy such as stents is frequently observed after implantation.[12–17] The *in vivo* fracture of the alloy is very complicated because of the interaction of several factors including corrosion, fatigue, fretting fatigue, wear and overload. Thus, the cause of the fracture must be determined to improve the reliability and safety of Ni-Ti superelastic alloy.

To simulate *in vivo* conditions, aqueous solutions containing hydrogen peroxide are sometimes used.[18–23] Hydrogen peroxide generated by an inflammatory response is considered to affect the corrosion behavior, surface conditions, or dissolution of ions of titanium and its alloys or Ni-Ti superelastic alloy.[18–23] However, there are no reports on corrosion due to hydrogen peroxide leading to fracture or the pronounced degradation of mechanical properties. If Ni-Ti superelastic alloy fractures associated with corrosion take place due to hydrogen peroxide, this is the first observation of such a process and the fracture may occur *in vivo*.

The corrosion behavior of Ni-Ti superelastic alloy has been investigated without applied stress in most cases.[6–11] On the other hand, we have demonstrated that when the applied stress exceeds the critical stress for martensite transformation, that is, the starting stress of the deformation because of the stress induction of B19′ martensite from the B2 parent phase,[5] general or localized corrosion is enhanced markedly in fluoride solutions[24] and sodium hypochlorite solutions,[25] eventually causing fracture. Hence, the applied stress possibly causes Ni-Ti superelastic alloy to fracture in the presence of hydrogen peroxide.

The objective of the present study is to investigate the fracture of sustained tensile-loaded Ni-Ti superelastic alloy in physiological saline solution contain-

*Correspondence to:* K. Yokoyama; e-mail: yokken@dent.tokushima-u.ac.jp
Contract grant sponsor: Ministry of Education, Culture, Sports, Science and Technology, Japan; contract grant numbers: 17791397, 15560632

TABLE I
Mechanical Properties and Transformation Temperatures of Tested Ni-Ti Superelastic Alloy

| | | | Transformation Temperature (°C) | | | |
|---|---|---|---|---|---|---|
| Critical Stress (MPa) | Tensile Strength (MPa) | Reduction in Area (%) | $A_f$ | $A_s$ | $M_s$ | $M_f$ |
| 542 ± 18.8 | 1255 ± 15 | 56.5 | 10.0 | −28.0 | 1.0 | −40.5 |

ing hydrogen peroxide. The findings will be helpful for the evaluation of the service life of improved Ni-Ti superelastic alloy in the future.

## EXPERIMENTAL

### Materials

Commercial Ni-Ti (Ni: 55 mass%, Ti: balance) superelastic alloy wires with a diameter of 0.50 mm were cut into 150-mm-long specimens. The specimens were carefully ground with 600-grit SiC paper and ultrasonically cleaned with acetone for 5 min. The phase transformation temperatures and mechanical properties of the specimens are listed in Table I. The phase transformation temperature of the specimens was determined by differential scanning calorimetry (DSC) according to the conventional method.[26] Prior to the DSC test, the specimens were maintained at 100°C. After reaching thermal equilibrium, the specimens were cooled to −50°C at a scan rate of 10°C/min. The same rate was used in heating the specimens to 100°C. Here, $M_s$ and $M_f$ indicate the start and finish temperatures for martensite transformation, respectively, on cooling. Similarly, $A_s$ and $A_f$ indicate the start and finish temperatures, respectively, for reverse transformation on heating. From stress–strain curves obtained by the tensile test, the critical stress for martensite transformation and the tensile strength were 542 and 1255 MPa, respectively. The tensile-test data were measured at room temperature [(25 ± 2)°C] using an Instron machine at a strain rate of $8.33 \times 10^{-4}$ $s^{-1}$. The standard deviation was calculated from the results of more than five specimens.

### Sustained tensile-loading test

A sustained tensile-loading test was carried out at room temperature with specimens 50-mm in length immersed in 50 mL of test solution. Applied stress was calculated as the ratio of the applied constant load to the initial cross-sectional area and was varied to determine fracture life characteristics, that is, time to facture versus applied stress. The test solution used was physiological saline solution containing hydrogen peroxide (0.15*M* NaCl + 0.3*M* $H_2O_2$) with pH of 5.5–6.0. Although this variation in pH seems to be difficult to avoid under aerated conditions, the effects of this variation in pH on the present experimental results were not detected. To prevent the light-assisted photodecomposition of hydrogen peroxide, the vessel of the test solution was covered with aluminum foil. Under the present experimental conditions, however, the concentration of hydrogen peroxide probably decreases with increasing immersion time. Hence, experimental results for long-term immersion should be discussed with caution. Immediately after fracture, the specimens were taken from the solution, cleaned with acetone, and dried in ambient air. The test was terminated when no fracture occurred after more than 1000 h. Fractography was performed by scanning electron microscopy (SEM). The area of the fracture surface associated with localized corrosion was measured from SEM images.

### Corrosion test

The corrosion potential of the specimens with or without applied stress was measured at room temperature in the test solution under aerated conditions. The counter electrode and reference electrode used were a platinum electrode and a saturated calomel electrode (SCE), respectively. The measurement was started 10 s after immersion in the test solution. The amounts of nickel and titanium ions dissolved in the test solution during immersion tests without the applied stress were analyzed by inductively coupled plasma (ICP) spectroscopy. Standard deviation was calculated from the results of 3–5 specimens.

### Surface analysis

The morphology of the side surface of the immersed specimens was examined by SEM. A surface chemical analysis of the immersed specimens without the applied stress for 24 h was performed by X-ray photoelectron spectroscopy (XPS) with Mg $K_\alpha$ radiation at 10 kV and 10 mA or Auger electron spectroscopy (AES) with a 30° takeoff angle and a 10 kV accelerating electron beam. The elemental depth profile of the surface layer on the specimens was determined by sputtering the layer using a scanning argon ion gun in AES. Argon ions were accelerated at an energy of 2 kV and a current of 30 mA, resulting in a sputtering rate of 15.4 nm/min calibrated for $SiO_2$. Oxide thickness was estimated from sputtering time for the oxygen peak to reach half its maximum concentration. This method, however, possibly overestimates the thickness of oxide on Ni-Ti alloy because of the higher density of $SiO_2$.[27]

## RESULTS

The sustained tensile-loading test results are plotted in Figure 1 in terms of the time to fracture as a function of applied stress in physiological saline so-

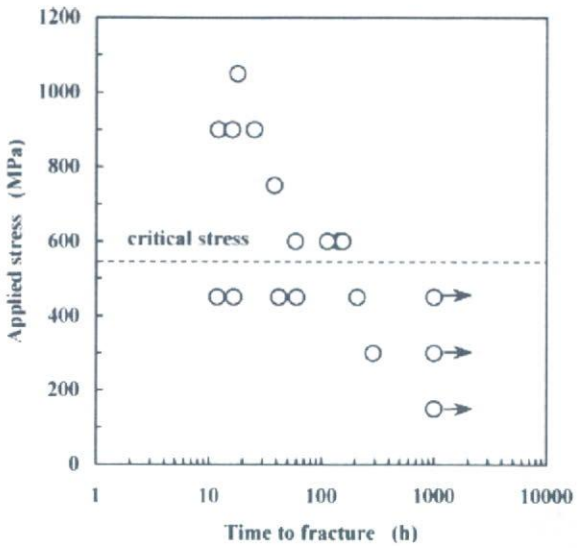


**Figure 1.** Time to fracture versus initial applied stress for Ni-Ti superelastic alloy immersed in physiological saline solution containing hydrogen peroxide.

lution containing hydrogen peroxide. The arrows in the figure denote data for nonfractured specimens at the indicated elapsed time. When the applied stress exceeded the critical stress for martensite transformation (542 MPa), fracture always occurred. In this stress range, the time to fracture was shorter than ~100 h and tended to decrease with increasing applied stress. Under an applied stress below 450 MPa, the alloy either fractured or did not fracture within 1000 h; the time to fracture tended to be longer than that above the critical stress for martensite transformation. In 0.3*M* $H_2O_2$ solution without NaCl, Ni-Ti superelastic alloy did not fracture within 1000 h even under an applied stress of 1050 MPa. No crevice corrosion resulted at the point of contact with the vessel in this experiment.

Figures 2(a–f) show fractographic features of the specimens that fractured in physiological saline solution containing hydrogen peroxide under applied stresses of 450 and 900 MPa. A slight reduction in area was observed under a high applied stress, whereas it was rarely observed under a low applied stress. The fracture surface was roughly classified into two areas: the corrosion area and the noncorrosion area with a mixture of quasi-cleavage and shallow dimples. Both areas were observed irrespective of the level of the applied stress. The fracture always initiated in the vicinity of the boundary between the corrosion and noncorrosion areas followed instantly by a radial crack propagation. The fracture initiation area could be identified by back tracking riverlike flows. A fraction of the corrosion area of the fracture surface as a function of the applied stress is shown in Figure 3. The fraction of the corrosion area tended to decrease with increasing applied stress. This result suggests that under a high applied stress (900 MPa), slight corrosion always results in fracture.

SEM images of the side surface of the specimens subjected to the sustained tensile-loading test in physiological saline solution containing hydrogen peroxide under applied stresses of 450 and 900 MPa are shown in Figures 4(a–d). The localized corrosion was observed only near the fracture area, but scratches due to paper polishing remained on the surface subjected no corrosion. The size of the localized corrosion area observed from the side surface of the specimens increased with decreasing applied stress. Under an applied stress below 450 MPa, the localized corrosion area was observed not only near the fracture area but also in other areas.

Figure 5 shows the changes in the corrosion potential of Ni-Ti superelastic alloy in physiological saline solution containing hydrogen peroxide with or without the applied stress. The corrosion potential was stable at ~0.2 V (vs. SCE) in the case without the applied stress. After 120 h of immersion, corrosion pits were observed on the surface of the specimen, although scratches due to paper polishing almost remained, as shown in Figure 6. In contrast, under the applied stress, the corrosion potential fluctuated at the early stage of immersion. Subsequently, the corrosion potential shifted abruptly in the less noble direction, corresponding to the fracture of the specimen, although it sometimes shifted to the noble direction without the fracture.

The amounts of nickel and titanium ions dissolved in physiological saline solution containing hydrogen peroxide without the applied stress after immersion are shown in Figure 7. The amounts of dissolved ions increased with immersion time, although the increase rate of amounts was slightly slowed down for long-term immersion. The amount of dissolved nickel ions was larger than that of dissolved titanium ions irrespective of immersion time. For 24 h, the amounts of dissolved nickel and titanium ions were 0.64 and 0.25 ppm, respectively.

Figure 8(a) shows typical Ti 2p XPS spectra of the nonimmersed specimen and specimen immersed in physiological saline solution containing hydrogen peroxide without applied stress for 24 h. The XPS spectra of the surface of both specimens exhibited two peaks at 458 and 463 eV, that is, Ti $2p_{1/2}$ and Ti $2p_{3/2}$ related to mainly $Ti^{4+}$ ($TiO_2$). Typical Ni $2p_{3/2}$ XPS spectra are shown in Figure 8(b). For the surface of the nonimmersed specimen, the peaks at 852 and 855 eV correspond to $Ni^0$ (nickel in the substrate metal) and $Ni^{2+}$ [$Ni(OH)_2$], respectively. For the immersed specimen, the peak related to $Ni^{2+}$ was observed, but no peak related to $Ni^0$ was observed.

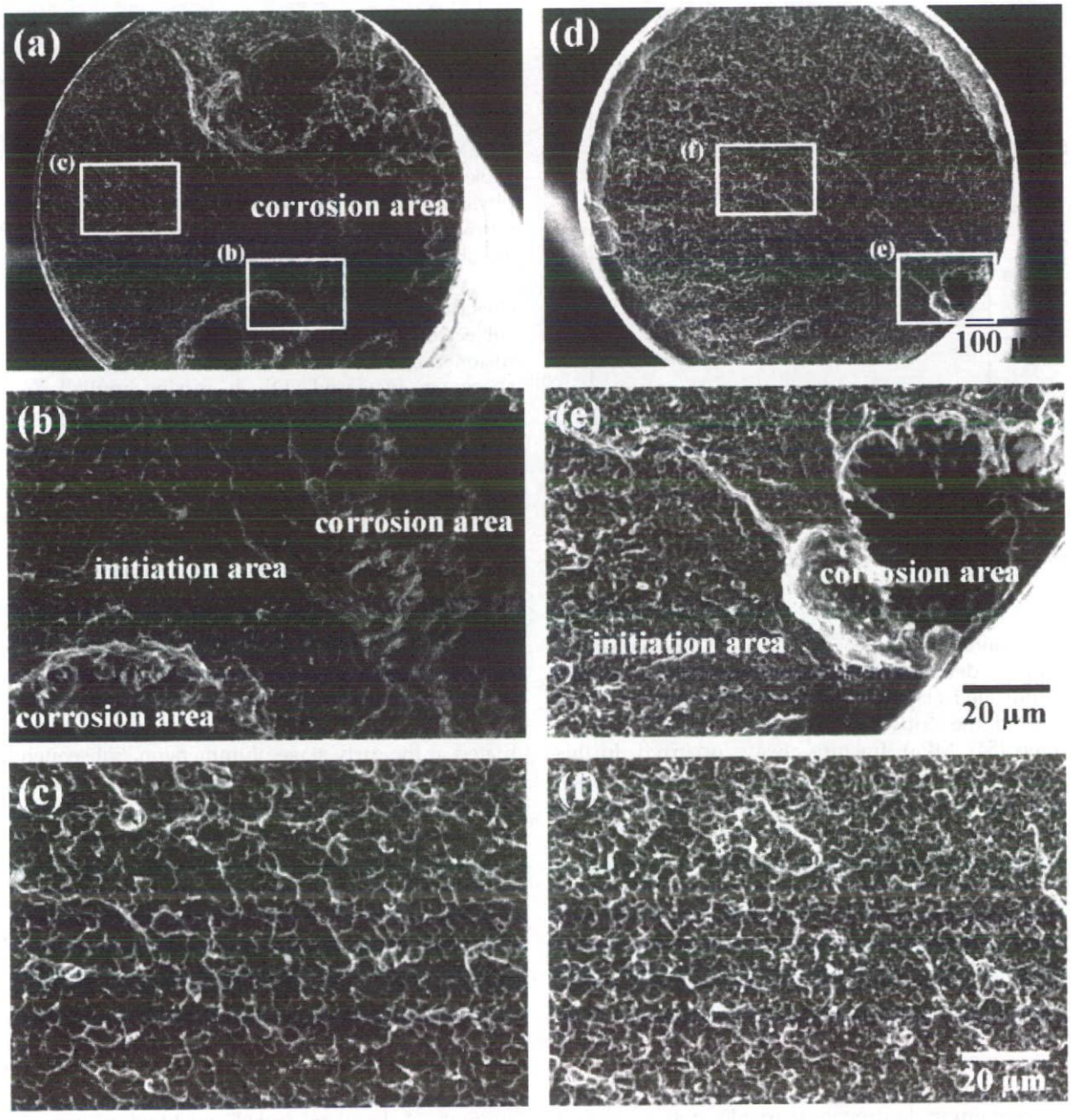


**Figure 2.** SEM images of typical fracture surface after sustained tensile-loading test in physiological saline solution containing hydrogen peroxide; (a) under applied stress of 450 MPa, (b) fracture initiation area and (c) crack propagation area, and (d) under applied stress of 900 MPa, (e) fracture initiation area and (f) crack propagation area.

Figures 9(a,b) show typical AES depth profile spectra of the nonimmersed specimen and specimen immersed in physiological saline solution containing hydrogen peroxide without applied stress for 24 h, respectively. For the nonimmersed specimen, the oxygen concentration decreased rapidly with sputtering time. In contrast, for the immersed specimen, the oxygen concentration decreased gradually with sputtering time. The oxide layer thicknesses of the nonimmersed and immersed specimens were roughly estimated to be 5 and 1000 nm, respectively. A decrease in relative nickel concentration was often observed in the oxide layer of the immersed specimen.

## DISCUSSION

One noteworthy finding in the present study is that Ni-Ti superelastic alloy fractures early under

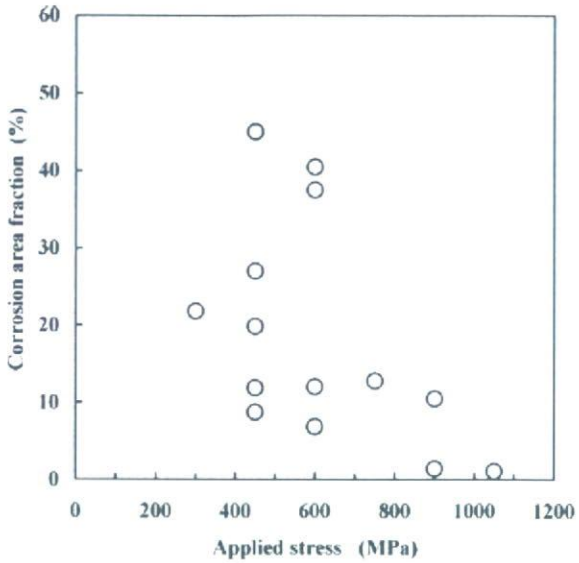


**Figure 3.** Fraction of corrosion area on fracture surface as function of applied stress.

applied stress in physiological saline solution containing hydrogen peroxide without fatigue or wear. Pan et al.[20] demonstrated that the presence of hydrogen peroxide enhances the dissolution of titanium and results in a rougher surface on the microscopic scale for commercial pure titanium immersed in phosphate-buffered saline solution. Montague et al.[28] reported that the presence of hydrogen peroxide enhances the fretting corrosion of Ti-6Al-4V alloy in cell culture growth media. Mu et al.[29] insisted that active oxygen species produced by macrophages lead to titanium ion release from commercial pure titanium in the absence of wear and fretting *in vivo*. Other articles[18–23,30–33] also exhibit the effects of hydrogen peroxide on corrosion resistance, surface conditions, or the dissolution of metal ions for titanium and its alloys. However, these reported effects of hydrogen peroxide are not anticipated to lead to a pronounced degradation of the mechanical properties or the fracture of titanium or Ni-Ti superelastic alloy for a short time. We have confirmed in a separate experiment that commercial pure titanium does not fracture within 1000 h under various applied stresses in physiological saline solution containing hydrogen peroxide.[34] Moreover, for Ni-Ti superelastic alloy without applied stress, slight-corrosion pits were observed only in physiological saline solution containing hydrogen peroxide, as shown in Figure 6.

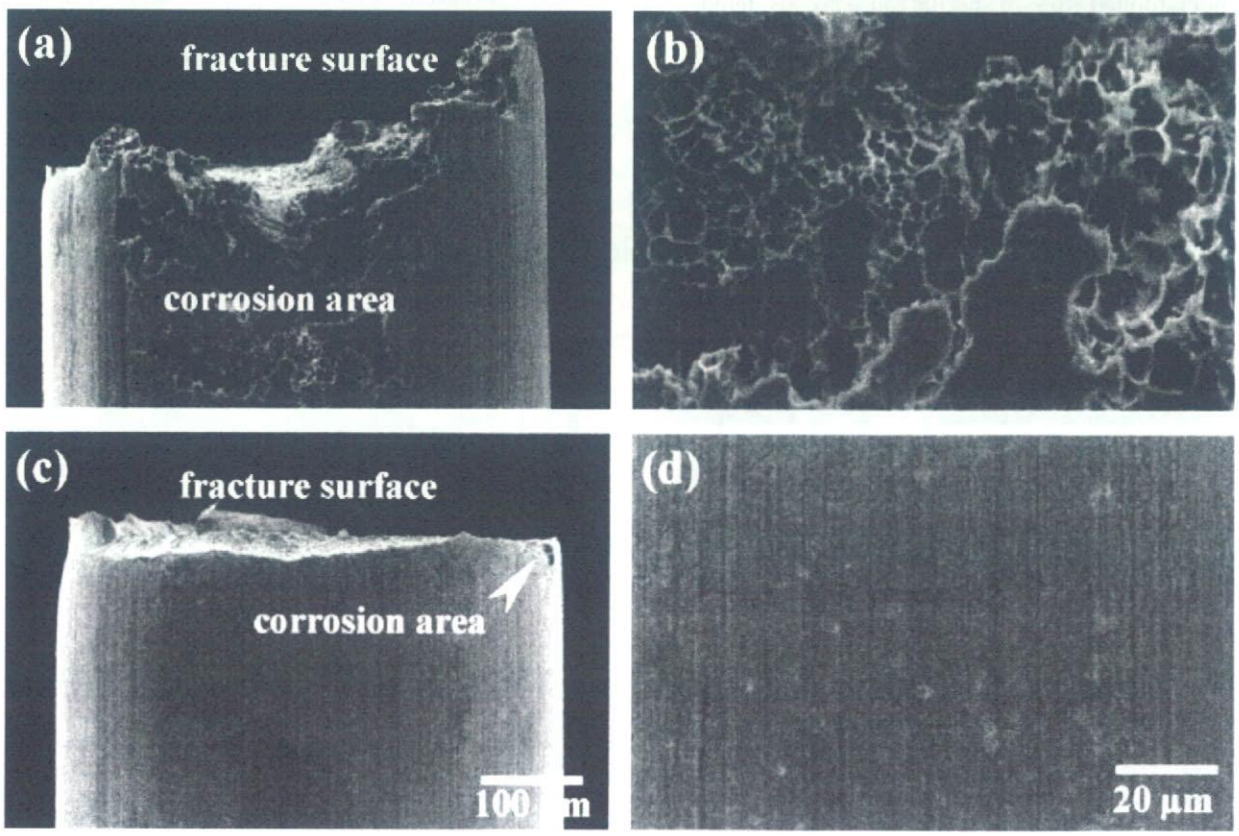


**Figure 4.** SEM images of typical side surface after sustained tensile-loading test in physiological saline solution containing hydrogen peroxide under applied stress of 450 MPa, (a) general and (b) magnified views; and under applied stress of 900 MPa, (c) general and (d) magnified views.

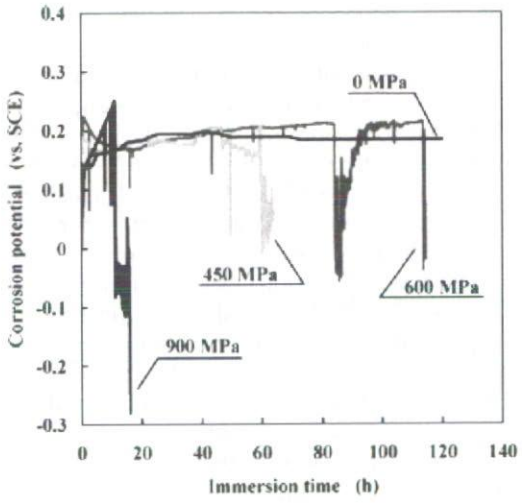


**Figure 5.** Changes in corrosion potential for various applied stresses in physiological saline solution containing hydrogen peroxide.

Although an increment in the amount of dissolved ions was observed even after 1000 h without applied stress (Fig. 7), this amount is not expected to lead to fracture. In regard to the fracture of Ni-Ti superelastic alloy under applied stress, a specific cause is considered.

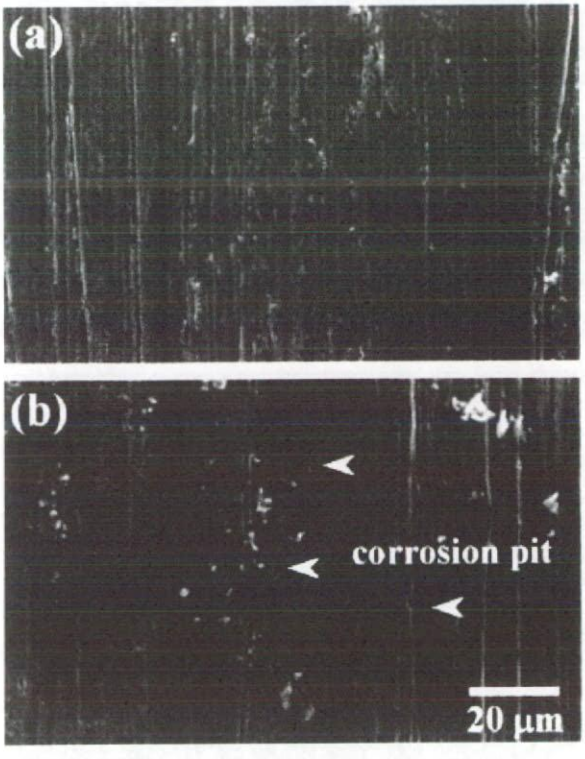


**Figure 6.** SEM images of side surface of (a) nonimmersed specimen and (b) specimen immersed in physiological saline solution containing hydrogen peroxide without applied stress for 120 h.

A few studies[35,36] showed that applied stress only slightly influences the corrosion resistance of Ni-Ti superelastic alloy in artificial saliva. As shown in Figure 5, however, a fluctuation in corrosion potential was observed at the early stage of immersion under applied stress. In addition, when the applied stress exceeded the critical stress for martensite transformation, the fracture of Ni-Ti superelastic alloy always occurred within a short time in physiological saline solution containing hydrogen peroxide, as shown in Figure 1. This result is consistent with those in fluoride solutions[24] and sodium hypochlorite solutions,[25] or under cathodic charging (applied potential) in physiological saline solution,[37] as reported previously. Under the present experimental conditions, it is most likely that fracture and corrosion behavior are markedly influenced by applied stress.

From the fractography (Fig. 2) and observation of the side surfaces (Fig. 4), the fracture of Ni-Ti superelastic alloy is presumably explained by overload due to localized corrosion in physiological saline solution containing hydrogen peroxide. However, the area of corrosion was smaller than that expected for the overload, as shown in Figure 3. In particular, in the high-applied-stress range, the fracture occurred because of the slight localized corrosion; hence, other fracture mechanisms such as stress concentration at fracture initiation areas may operate. Under an applied stress of 450 MPa, the fracture sometimes occurred within 100 h, similar to that under an applied stress above the critical stress for martensite transformation (542 MPa). The possible reason for this is that the reduction in the cross-

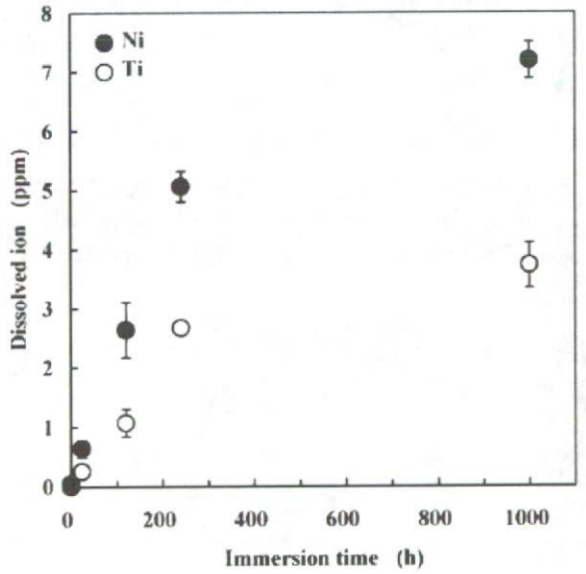


**Figure 7.** Amounts of dissolved nickel and titanium ions immersed in physiological saline solution containing hydrogen peroxide without applied stress.

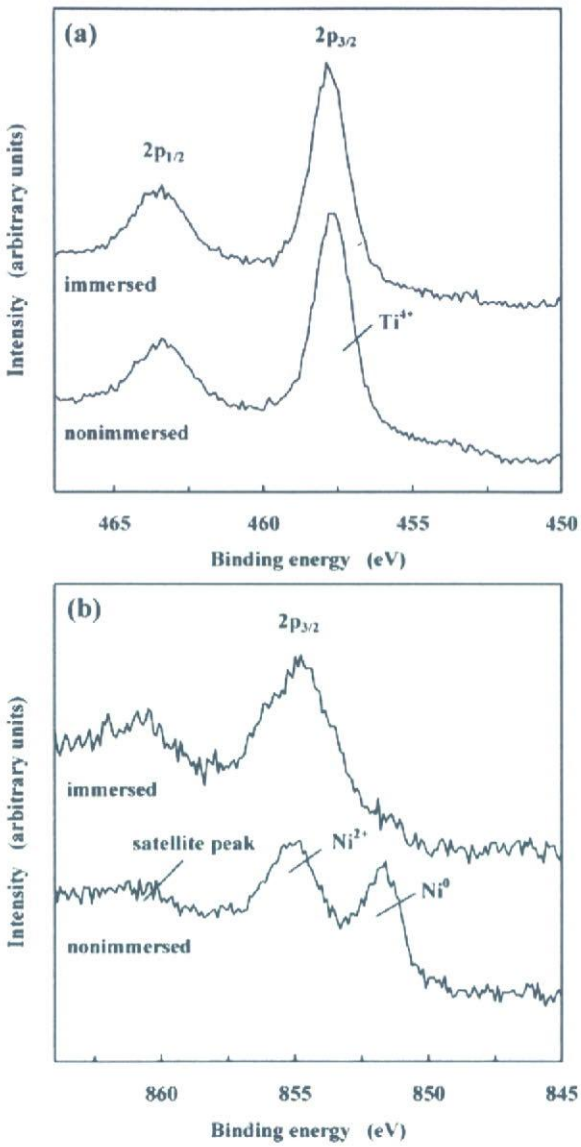


**Figure 8.** Typical XPS spectra of nonimmersed specimen and specimen immersed in physiological saline solution containing hydrogen peroxide without applied stress for 24 h: (a) Ti 2p and (b) Ni $2p_{3/2}$.

sectional area by slight localized corrosion results in the applied stress exceeding the critical stress for martensite transformation. Dynamic processes such as the stress-induced martensite transformation during the sustained tensile-loading test may enhance fracture.[38] The occurrence of localized corrosion also appears to lead to the wide scattering of the time to fracture.

In sodium hypochlorite solutions such as a disinfectant, the fracture of Ni-Ti superelastic alloy under applied stress is probably caused by localized corrosion associated with the preferential dissolution of nickel ions.[25] The preferential or selective dissolution of nickel ions for Ni-Ti superelastic alloy has been observed in various environments.[2,9,39] Similarly, the present results of ICP (Fig. 7), XPS (Fig. 8), or AES (Fig. 9) indicate the preferential dissolution of nickel ions in physiological saline solution containing hydrogen peroxide. Additionally, we have observed in a separate experiment that pure nickel (99.9%) fractures under applied stress in physiological saline solution containing hydrogen peroxide.[40] In this case, general corrosion rather than localized corrosion is observed, suggesting that nickel readily dissolves in physiological saline solution containing hydrogen peroxide. The time to fracture of pure nickel wire with a diameter of 0.50 mm was relatively long (~800 h) despite the applied stress of around the yield stress (300 MPa). The difference in corrosion morphology, that is, the difference in fracture mechanism, probably affects the time to fracture. The

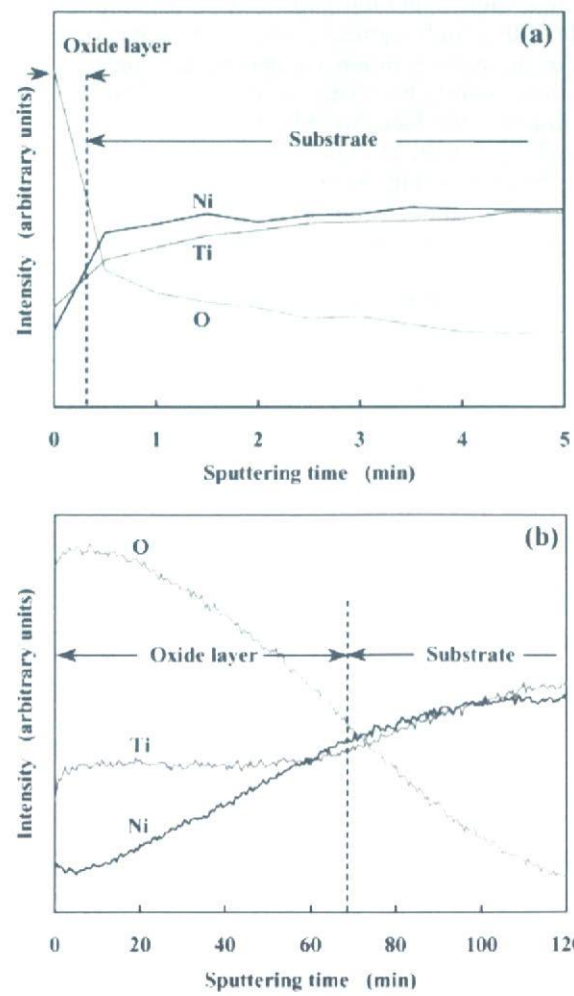


**Figure 9.** Typical AES depth profile of (a) nonimmersed specimen and (b) specimen immersed in physiological saline solution containing hydrogen peroxide without applied stress for 24 h.

relation between corrosion behavior and fracture mechanism will be published elsewhere. In contrast, commercial pure titanium slightly dissolves as mentioned earlier. Hence, it is likely that the localized corrosion of Ni-Ti superelastic alloy in physiological saline solution containing hydrogen peroxide is induced by the preferential dissolution of nickel ions.

In hydrogen peroxide solution without sodium chloride, Ni-Ti superelastic alloy did not fracture within 1000 h even under an applied stress above the critical stress for martensite transformation. This finding is in accord with the fact that the corrosion resistance of titanium and Ni-Ti alloys covered with mainly titanium oxide film is generally sensitive to chloride ions.[41] However, there is no report on Ni-Ti superelastic alloy under sustained load fracturing in physiological saline solution without other solutes. The localized corrosion in the present study perhaps results from synergistic effects of hydrogen peroxide with a high oxidation capability and sodium chloride with a high aggressiveness to induce corrosion.

An aqueous solution containing hydrogen peroxide has recently been employed in surface treatments to improve the biocompatibility of Ni-Ti superelastic alloy[42–45] as well as titanium and its alloys.[31,46–49] As shown in XPS (Fig. 8) or AES (Fig. 9), an increment in oxide thickness and a decrease in nickel in the oxide layers were observed for the immersed specimen. Chu et al.[45] reported that Ni-Ti shape memory alloy in boiling hydrogen peroxide solution without other solutes forms a titania scale, which is mainly composed of rutile and anatase phases and is relatively deficient in nickel. As long as hydrogen peroxide solutions without other solutes such as sodium chloride are used in the absence of applied stress, no pronounced degradation of mechanical properties may occur on the basis of the results of the present study.

For *in vitro* investigation, the concentrations of hydrogen peroxide used for simulating inflammatory responses have ranged from 0.001 to 0.330*M*.[18–20,22,28,30] In the present study, the initial hydrogen peroxide concentration was 0.3*M*. However, hydrogen peroxide is decomposed readily into water and molecular oxygen according to

$$2H_2O_2 \rightarrow 2H_2O + O_2,$$

which is catalyzed by the presence of $TiO_2$ on the surface of Ni-Ti superelastic alloy. Under the present experimental conditions, hydrogen peroxide concentration probably decreased with increasing immersion time, although the decomposition rate of hydrogen peroxide was not known. This is supported by the fact that the increment in amounts of dissolved ions decreased slightly after 1000 h, as shown in Figure 7. Nevertheless, it should be noted that the fracture occurred after long-term immersion under an applied stress below 450 MPa. In this case, it appears that the fracture occurred after reducing the concentration of hydrogen peroxide. Therefore, the critical hydrogen peroxide concentration for the fracture of Ni-Ti superelastic alloy is lower than 0.3*M* and should be investigated.

There are several differences between the present experimental conditions and *in vivo* conditions. The test solution temperature was 25°C in the present study, which became the baseline value. Because corrosion is generally enhanced by the temperature of the environment, the time to fracture at 37°C would become shorter than that at 25°C. Dissolved oxygen and pH also influence corrosion behavior. The diameter of the present specimen is one order of magnitude larger than that of a stent strut. With decreasing diameter of the specimen, the time to fracture generally reduces in the case of fracture because of the localized corrosion. The surface conditions of the specimen affect corrosion resistance. The applied stress level should be treated cautiously. Ni-Ti superelastic devices are usually used within the superelastic strain (corresponding to the applied stress below 542 MPa), although the applied stress possibly exceeds the critical stress for martensite transformation. In many cases, sustained strain tests reflect practical conditions rather than sustained loading tests. Dynamic processes including phase transformation, as compared with sustained loading, are considered to enhance fracture.[38] Other factors should also be considered.

It must be emphasized that Ni-Ti superelastic alloy under applied stress possibly fractures because of the hydrogen peroxide *in vivo*. In fact, *in vivo*, the fracture of Ni-Ti superelastic alloy such as stent is frequently observed from a few months to a few years after implantation.[12–17] Using energy-dispersive X-ray analysis, Heintz et al.[12] revealed corrosion pits and localized corrosion on the surface of nitinol stent wires of explanted endovascular grafts used for the treatment of abdominal aortic aneurysm, and a decrease in nickel concentration in localized corrosion areas. Although the differences between *in vivo* and *in vitro* should be treated carefully, the morphology of corrosion *in vivo*[12] appears to resemble closely that in the present study. One reason for the fracture of Ni-Ti superelastic alloy *in vivo* may be localized corrosion due to the synergistic effects of hydrogen peroxide and sodium chloride under applied stress. Further works are needed to clarify this.

## CONCLUSIONS

We have demonstrated that Ni-Ti superelastic alloy fractures under applied stress in physiological